

# Highly Active Cellulose-Supported Poly(hydroxamic acid)–Cu(II) Complex for Ullmann Etherification

Choong Jian Fui, Tang Xin Ting, Mohd Sani Sarjadi, Zarina Amin, Shaheen M. Sarkar, Baba Musta, and MdLutfur Rahman\*



Cite This: *ACS Omega* 2021, 6, 6766–6779



Read Online

ACCESS |



Metrics & More

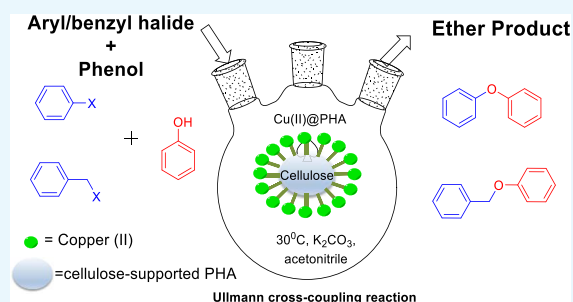


Article Recommendations



Supporting Information

**ABSTRACT:** Highly active natural pandanus-extracted cellulose-supported poly(hydroxamic acid)–Cu(II) complex **4** was synthesized. The surface of pandanus cellulose was modified through graft copolymerization using purified methyl acrylate as a monomer. Then, copolymer methyl acrylate was converted into a bidentate chelating ligand poly(hydroxamic acid) via a Loosen rearrangement in the presence of an aqueous solution of hydroxylamine. Finally, copper species were incorporated into poly(hydroxamic acid) via the adsorption process. Cu(II) complex **4** was fully characterized by Fourier transform infrared (FTIR), field emission scanning electron microscopy (FE-SEM), energy-dispersive X-ray (EDX), transmission electron microscopy (TEM), inductively coupled plasma optical emission spectrometry (ICP-OES), thermogravimetric analysis (TGA), X-ray diffraction (XRD), and X-ray photoelectron spectroscopy (XPS) analyses. The cellulose-supported Cu(II) complex **4** was successfully applied (0.005 mol %) to the Ullmann etherification of aryl, benzyl halides, and phenacyl bromide with a number of aromatic phenols to provide the corresponding ethers with excellent yield [benzyl halide (70–99%); aryl halide (20–90%)]. Cu(II) complex **4** showed high stability and was easily recovered from the reaction mixture. It could be reused up to seven times without loss of its original catalytic activity. Therefore, Cu(II) complex **4** can be commercially utilized for the preparation of various ethers, and this synthetic technique could be a part in the synthesis of natural products and medicinal compounds.



## 1. INTRODUCTION

The copper-catalyzed Ullmann coupling reaction is a crucial strategy in the development of a C–O bond where the reaction has significant importance in the pharmaceutical, agrochemical, and polymer industries.<sup>1–3</sup> Conventionally, the Ullmann-type C–O bond formation reaction is carried out through electron-pair donors, phenols with aryl halides. However, this reaction suffers from several disadvantages, such as requiring high temperature, moderate yield (30–50%), prolonged reaction time, and excessive usage of copper catalysts that limit its extensive applications.<sup>4,5</sup> Therefore, various metal-based catalysts, such as palladium, nickel, and gold, along with various stabilizing chelating ligands, have been explored and examined for the C–O bond formation to overcome these issues.<sup>6</sup> Unfortunately, these metal-based catalysts face several drawbacks; for example, they are expensive, highly toxic, and usually involve poisonous organic phosphines as a stabilizing ligand.<sup>7</sup> In the past decade, therefore, many researchers have shifted their focus toward the copper-catalyzed C–O bond formation by the utilization of N/O-donor or P-based ligands, such as neocuproin, phenanthroline, amino glycerin, tripodal ligands, PPAPM, diimine derivatives, niacin, diamine derivative-based silica compound, *N,N*-dimethyl biguanide, and quinoxaline oxide analogs.<sup>4</sup> However, to achieve a higher

yield of ether, these ligands have been utilized under homogeneous reaction conditions, which have several drawbacks, e.g., contamination of products and the inability to regenerate the catalyst.<sup>4</sup> However, electrostatic interaction and hydrogen bonds between stabilizers and metal ions play a vital role in preventing the growth and accumulation of metal in the reaction media.<sup>8,9</sup> Currently, most researchers have focused on utilization of eco-friendly, renewable resources and sustainable solid supports and processes that apply to tangible assistance.<sup>10</sup> The solid-supported catalysts, namely, metal-organic framework/covalent organic framework (MOF/COF)-supported,<sup>11,12</sup> polystyrene-supported,<sup>13</sup> nonmagnetic- and magnetic-supported,<sup>14</sup> carbon-based,<sup>15</sup> MCM-supported,<sup>16</sup> metal-decorated hyper-cross-linked network,<sup>17</sup> and salen-based hyper-cross-linked polymer catalysts,<sup>18,19</sup> showed an extraordinary catalytic ability toward the organic reaction. Nevertheless, they are out of the viewpoint of sustainable protocols in green

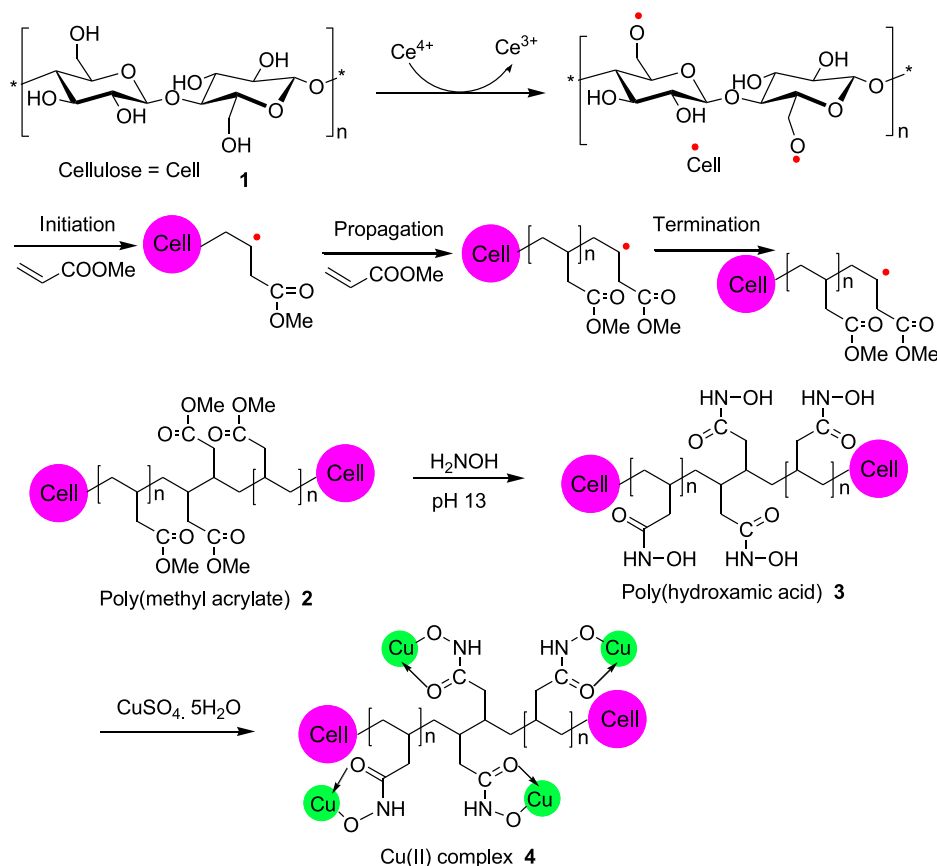
Received: December 1, 2020

Accepted: February 8, 2021

Published: March 5, 2021



Scheme 1. Preparation of Cu(II) Complex 4



chemistry principles. By considering sustainable protocols, natural polymers are more suitable as solid supports in the synthesis of heterogeneous catalysts. The natural polymers including alginate,<sup>20</sup> gelatin,<sup>21</sup> starch,<sup>22</sup> chitosan,<sup>23</sup> and cellulose<sup>10,24,25</sup> have been utilized as solid support for catalytic reactions. In recent years, cellulose-supported adsorbents utilized as a catalyst have gained significant interest due to their biodegradability, abundance in nature, eco-friendly characteristics, water insolubility, and cost-effectiveness.<sup>25,26</sup> The pure cellulose has inadequate metal species sorption capacity, which can be improved by chemical modification of the cellulose backbone. Based on previous studies, introducing a functional group, such as carboxyl, amine, and sulfur groups, onto the surface of cellulose can dramatically improve the metal-binding capacity.<sup>27–32</sup> In addition, most researchers have been focusing on exploring a new type of ligand to functionalize the cellulose surface, which has a profound impact on the catalytic ability with low leaching of metal species.<sup>10</sup>

Recently, several studies reported, such as functionalized waste corn-cob cellulose-supported copper nanoparticles for *N*-alkylation reaction of amines;<sup>33</sup> a cellulose-supported palladium catalyst for the Heck, Ullmann, and Sonogashira coupling reaction;<sup>34–37</sup> a cellulose-supported copper catalyst for aza-Michael addition and click reactions;<sup>38–40</sup> functionalized cellulose with several binding sites;<sup>10</sup> and 2-aminopyridine functionalized,<sup>41</sup> *N*-methylimidazole functionalized,<sup>25</sup> *N*-heterocyclic carbene functionalized hydroxyethyl,<sup>9</sup> and amine functionalized<sup>42</sup> cellulose-supported palladium complex catalysts, have been used for the Suzuki reaction. However, only a few studies have been found where cellulose-

supported copper catalysts were used for the Ullmann cross-coupling reaction.

Herein, we report a cellulose-supported poly(hydroxamic acid)-functionalized copper catalyst for the Ullmann etherification reaction. In this report, we anchored the Cu(II) nanocomplex onto pandanus cellulose-supported poly(hydroxamic acid) as an efficient heterogeneous catalyst for carbon–oxygen bond (C–O) formation through the Ullmann etherification reaction. The cellulose-supported Cu(II) nanocomplex exhibited excellent catalytic activity in C–O bond formation reactions of various aryl/benzyl and phenacyl halides with phenols. The Cu(II) nanocomplex was easy to separate from the reaction medium and could be recycled up to seven times without any substantial loss of its catalytic activity.

## 2. RESULTS AND DISCUSSION

### 2.1. Synthesis of Cellulose-Supported Poly(hydroxamic acid) Cu(II) Complex 4.

The easiest way to modify the cellulose surface is to add new functional groups onto the cellulose backbone.<sup>43</sup> First, the pulp was hydrolyzed into cellulose I to increase the number of hydroxyl groups on the cellulose surface.<sup>44</sup> Then, –OH functional groups on the cellulose surface were converted into oxygen radicals using cerium(IV) ammonium nitrate as an initiator. The ceric salt acts as an oxidizing agent for an oxidative addition reaction of electrophilic radicals. The hydrogen atom of the –OH group was removed by the reduction of the oxidation state +4 to +3 for the ceric ion (Scheme 1).

Then, the radical present on the oxygen undergoes initiation of the grafting process by linking with the methyl acrylate

monomer. Further radical formation leads to the propagation reaction. At the termination stage, the growing polymer chains were reacted together to produce grafted poly(methyl acrylate) **2**. Further, the methyl acrylate functional group in **2** is reacted with an aqueous solution of hydroxylamine through a Loosen rearrangement to obtain the corresponding bidentate chelating ligand poly(hydroxamic acid) **3**. Earlier studies reported that hydroxamic acid is an effective ligand to adsorb copper metal.<sup>32,45</sup> Therefore, we treated poly(hydroxamic acid) **3** with an aqueous solution of copper sulfate at room temperature to obtain a five-membered Cu(II) complex **4** (Scheme 1). In compliance with the Eigen and Tamm study, the formation of the complex structure was begun with the formation of an electrostatic ion pair between the metal ions and the chelating ligand.<sup>46</sup>

**2.2. Infrared Spectroscopy Analysis.** The Fourier transform infrared (FTIR) spectra of the materials investigated in this study are presented in Figure 1. A comparison was made between the pandanus cellulose (cellulose **1**), poly(methyl acrylate) **2**, poly(hydroxamic acid) **3**, and Cu(II) complex **4**.

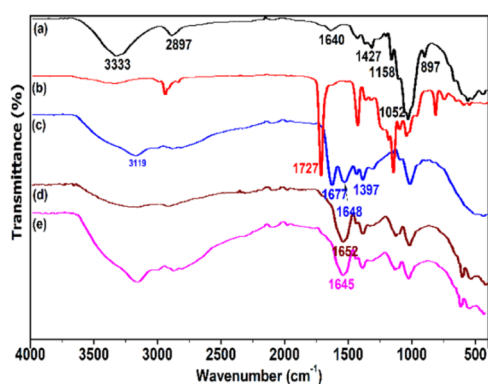


**Figure 1.** FTIR spectra of (a) cellulose **1**, (b) poly(methyl acrylate) **2**, (c) poly(hydroxamic acid) **3**, (d) Cu(II) complex **4**, and (e) Cu(II) complex **4** after the seventh cycle of reaction.

The IR spectrum of cellulose **1** showed an absorption peak at 3333 and 1427  $\text{cm}^{-1}$ , indicating the stretching and bending mode of  $-\text{OH}$ . An absorption band for the  $\text{Sp}^3$  C–H stretching mode was observed at 2897  $\text{cm}^{-1}$  (Figure 1a), which was also reported in earlier studies.<sup>47,48</sup> A bending mode at 1640  $\text{cm}^{-1}$  was observed from the water molecule that bound to the cellulose surface. A small sharp peak at 1158  $\text{cm}^{-1}$  is attributed to the C–O stretching of the glycosidic unit in cellulose.<sup>47</sup> The vibration of the hemiacetal structure of cellulose and the skeletal C–O–C pyranose ring in the cellulose can be observed at 1052  $\text{cm}^{-1}$ . A small sharp peak at 897  $\text{cm}^{-1}$  belongs to the glycosidic  $\text{C}_1\text{–H}$  distortion with the bending of the O–H bond indicating the association of  $\alpha$ -glycoside between the glucose units.<sup>47</sup>

The spectrum of grafted poly(methyl acrylate) **2** showed a new strong peak at 1727  $\text{cm}^{-1}$  due to the carbonyl group in the methyl acrylate monomer (Figure 1b). All of the remaining peaks were found to be similar to those of the peaks for cellulose **1** (Figure 1a).<sup>47,48</sup> This result confirms that methyl acrylate with the C=O functional group was successfully grafted onto the surface of the cellulosic material.

However, in poly(hydroxamic acid) **3**, the stretching of C=O at 1727  $\text{cm}^{-1}$  (Figure 1b) was shifted toward a lower wavenumber at 1677  $\text{cm}^{-1}$  (Figure 1c), which indicated that

the ester moieties in grafted poly(methyl acrylate) **2** were converted into a hydroxamic acid **3**.<sup>47,48</sup> A new peak was also observed at 1648  $\text{cm}^{-1}$ , attributed to the bending mode of the N–H group. A broad band appeared at 3119  $\text{cm}^{-1}$  due to the overlap of the O–H and N–H stretching modes.

The IR spectrum of Cu(II) complex **4** showed that the carbonyl group was further shifted from 1677  $\text{cm}^{-1}$  (polymer **2**) to 1652  $\text{cm}^{-1}$  due to the coordination of Cu(II) with the hydroxamic acid chelating ligand (Figure 1d). Additionally, the peak at 3119  $\text{cm}^{-1}$  for N–H stretching was also affected due to the complex formation with Cu(II). This result indicates that the copper metal was successfully adsorbed onto the chelating ligand, yielding the pandanus cellulose-supported poly(hydroxamic acid) Cu(II) complex **4**. After seven cycles of the Ullmann reaction, the IR spectrum of Cu(II) complex **4** was similar to that of fresh Cu(II) complex **4**, indicating that poly(hydroxamic acid) was strongly coordinated with Cu(II) (Figure 1e).

**2.3. Field Emission Scanning Electron Microscopy (FE-SEM) Analysis.** FE-SEM micrograph of raw pandanus fiber showed substantial impurities, as shown in Figure S2ai,aii. A chemical treatment was utilized to remove several constituents such as lignin, glucomannans, xylans, extractives, ash, etc. The pandanus cellulose pulp showed a noticeably smooth wooden sticklike structure (lower and higher magnification presented in Figure S2bi,bii, respectively). Hydrolyzed cellulose **1** showed a slightly different morphology (Figure 2a; higher magnification presented in Figure S2c). The cellulose pulp and cellulose **1** differed in size and shape, where the pandanus cellulose pulp had a wooden sticklike structure and cellulose **1** showed a spherelike structure with a smaller size.

Poly(methyl acrylate) **2** showed a rough surface with a deformed spherelike morphology. As a result, cellulose **1** underwent a successful graft-copolymerization reaction (Figure 2b; higher magnification presented in Figure S2d). In poly(hydroxamic acid) **3**, an unsmooth structural surface with a distinguishable small sphere shape was observed (Figure 2c; higher magnification presented in Figure S2e). However, Cu(II) complex **4** showed a smaller compact spherical morphology compared to poly(hydroxamic acid) **3** due to the complexation between amidoxime and copper species (Figure 2d; higher magnification presented in Figure S2f). Interestingly, after the seventh cycle of the Ullmann reaction, the SEM image of Cu(II) complex **4** also showed a spherical morphology (Figure 2e at a higher magnification). This result suggested that Cu(II) complex **4** was stable in the reaction media and that copper species were not aggregated during the reaction.

**2.4. Transmission Electron Microscopy (TEM) Analysis.** The TEM analysis of Cu(II) complex **4** was carried out on a Tecnai G2 Spirit BioTwin transmission electron microscope, using a 200 mesh copper grid coated with carbon film at 120 kV. The TEM analysis showed that the presence of copper nanoparticle complexes on the pandanus cellulose-supported poly(hydroxamic acid) surface (Figure 3a), and the size of the average complex was  $\varnothing = 33.7 \pm 2$  nm (Figure 3c). The size of copper on complex **4** determined by TEM is associated with the value of the X-ray diffraction (XRD) mean crystal size calculated by the Scherrer equation as 33.7 and 33.1 nm. The copper nanocomplex exhibited a spherical morphology with a random distribution of copper species on the cellulose surface (Figure 3a). We also examined the TEM

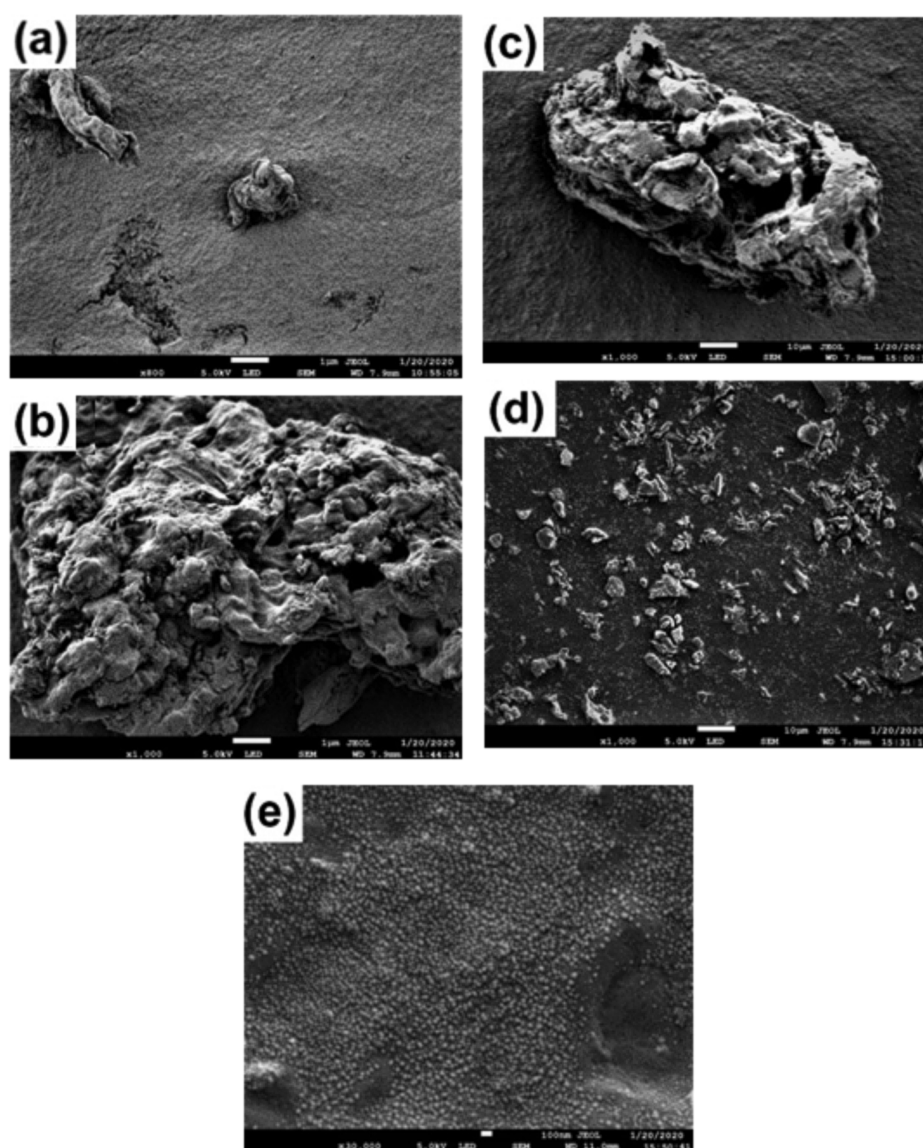


**Figure 2.** SEM of (a) cellulose 1, (b) poly(methyl acrylate) 2, (c) poly(hydroxamic acid) 3, (d) Cu(II) complex 4, and (e) Cu(II) complex 4 after the seventh cycle reaction.

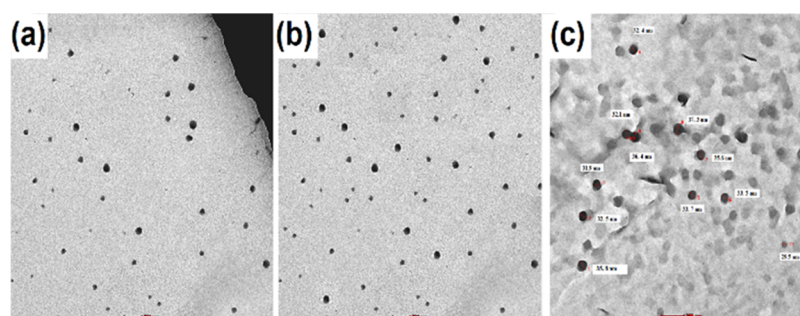


**Figure 3.** TEM image of (a) fresh Cu(II) complex 4 and (b) Cu(II) complex 4 after the seventh cycle reaction (c) measurement.

image of Cu(II) complex 4 after the seventh cycle of the Ullmann reaction. The TEM image of reused Cu(II) complex 4 showed similar morphology, as well as similar distribution with the same spherical diameter (Figure 3b). Therefore, the TEM image again revealed that during the Ullmann reaction, Cu(II) complex 4 showed high stability and copper species were not aggregated.

**2.5. Energy-Dispersive X-ray (EDX) Analysis.** Figure 4 presents the EDX spectra of Cu(II) complex 4. The EDX spectra also indicated the presence of copper species (8.03 keV), and it was estimated that 35.4% of copper species was incorporated in Cu(II) complex 4.

**2.6. Thermogravimetry Analysis.** Thermogravimetric analysis is a conventional method that provides evidence for

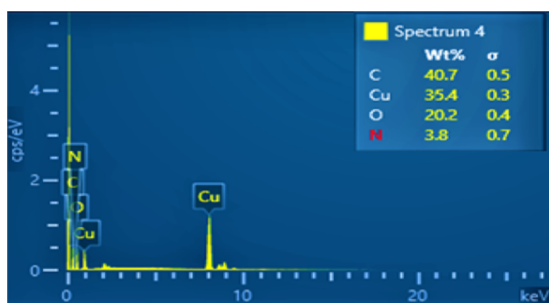


Figure 4. EDX image of Cu(II) complex 4.

the formation of a new substance<sup>49</sup> and is frequently used to determine the thermal stability of materials.<sup>50</sup> The thermal behavior of pandanus cellulose 1, poly(methyl acrylate) 2, poly(hydroxamic acid) 3, and Cu(II) complex 4 was studied with a heating rate of 15 min<sup>-1</sup> in a nitrogen atmosphere, and the thermogravimetric analysis (TGA) results are presented in Figure 5. In the complete analysis, several changes were

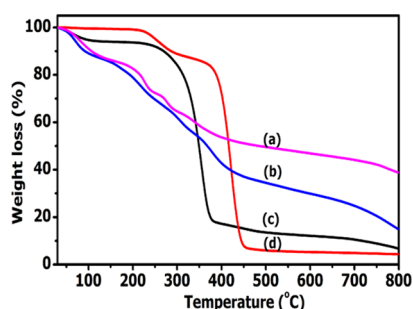


Figure 5. TG graphs of (a) Cu(II) complex 4, (b) poly(hydroxamic acid) 3, (c) cellulose 1, and (d) poly(methyl acrylate) 2.

observed for these materials at different temperatures. A small weight loss was noticed for all materials below 100 °C. This may have resulted from the evaporation of the remaining water and the volatile organic solvent (methanol, acetone, etc.), which are located at the external and internal cavities of cellulose 1 (6%), poly(methyl acrylate) 2 (2%), poly(hydroxamic acid) 3 (11%), and Cu(II) complex 4 (9%). The high-water content in poly(hydroxamic acid) 3 confirms that it has hydrophilic properties. The TGA curve of cellulose 1 showed a significant weight loss from 315 to 390 °C due to the degradation of molecule fragments such as the -OH and -CH<sub>2</sub>OH groups that are located on the cellulose surface (Figure 5c).<sup>51</sup>

Poly(methyl acrylate) 2 has two stages of degradation within a temperature range of 210–500 °C (Figure 5d). The first weight loss (~12%) occurs between 215 and 310 °C due to the dehydrogenation<sup>51</sup> and degradation of the grafted ester group. The second stage of weight loss (~81%) starts in the range of 390–460 °C and could be due to the degradation of the remaining methyl acrylate chain. The first small degradation and second large degradation of the curve prove that a large amount of methyl acrylate is grafted on cellulose. Based on the study of Fernández et al., the thermal stability of graft copolymer decreases with an increase of the percent grafting yield. Besides, a high grafting yield has a small degradation in the range of 200–350 °C, followed by significant degradation in the range of 310–460 °C.<sup>52,53</sup> Based on this result, the thermal stability curve of polymer 2

was associated with the findings of Fernández, and this can prove that a high percent grafting yield occurred on the surface of cellulose.

Poly(hydroxamic acid) 3 has four stages of a continuous small degradation in the temperature range of 140–470 °C (Figure 5b). This degradation was owing to the degradation of the hydroxamic acid and the cellulose functional group. An intersection point between poly(methyl acrylate) 2 and poly(hydroxamic acid) 3 occurs at around 450 °C. After this point, poly(hydroxamic acid) 3 remained stable, while poly(methyl acrylate) 2 continued to degrade until 500 °C and then remained stable (Figure 5b,d). The total weight loss of poly(hydroxamic acid) 3 is 65% while that of poly(methyl acrylate) 2 is 80%. Cu(II) complex 4 is more stable than poly(hydroxamic acid) 3 at 425 °C cross-point and the weight loss was found to be 50% at 550 °C (Figure 5a), whereas 70 and 90% losses were found for poly(hydroxamic acid) 3 and poly(methyl acrylate) 2, respectively (Figure 5b,d). Overall, poly(hydroxamic acid) 3 and Cu(II) complex 4 had better stability than their precursors, which is good behavior in terms of thermal degradation of the final products.

**2.7. X-ray Diffraction (XRD) Analysis.** The X-ray diffraction patterns were obtained with a Rigaku automated multipurpose X-ray diffractometer, using Cu K $\alpha$  at 40 kV and 50 mA. Scattered radiation was detected in the range of  $2\theta = 3\text{--}80^\circ$  at a scan rate of  $4^\circ/\text{min}$ . The XRD analysis results are shown in Figure 6, and the crystalline index (CrI) is calculated according to the Segal empirical method described in the following equation (eq 1)<sup>54</sup>

$$\text{CrI} = \frac{A_{\text{crystalline}}}{A_{\text{amorphous}} + A_{\text{crystalline}}} \times 10 \quad (1)$$

where  $A_{\text{amorphous}}$  is the area under the amorphous curve and  $A_{\text{crystalline}}$  is the area under the sample curve.

XRD diffraction patterns of cellulose 1 were recorded at  $2\theta = 15.43, 22.65, \text{ and } 34.40^\circ$ , which are characteristic peaks for cellulose, corresponding to the lattice planes 110, 200, and 004, respectively (Figure 6a).<sup>55,56</sup> The major crystalline peak was observed at  $22.65^\circ$  with an intensity of 100%, which confirms the crystallinity of cellulose.<sup>57</sup> The intensity of the pattern of the untreated pandanus fruit fiber was reduced and the crystallinity index was just 35.3%, indicating the presence of amorphous substances in the pandanus fruit fiber. Due to the decreasing number of noncellulosic substances, the peak pattern of cellulose 1 became narrower and the crystallinity index increased from 35.3 to 78.2%. This high CrI indicates the removal of the amorphous phase and the excellent mechanical properties of the cellulose from the pandanus fruit fiber.<sup>55–58</sup>

To further illustrate the influence of polymerization on cellulose, the XRD pattern of poly(methyl acrylate) 2 is presented in Figure 6bii. Except for a new diffraction peak at about  $7, 11, 12.8, \text{ and } 17^\circ$ , and a slight change in the diffraction intensity, the XRD pattern of poly(methyl acrylate) 2 was almost the same as that of cellulose 1. This result may suggest that the ordered structure of cellulose was not changed after the grafting, and new diffraction peaks were observed from the methyl acrylate chains. It should be noted that after copolymerization, the cellulose surface becomes soft and rubbery, indicating that graft copolymerization had occurred on the cellulose surface. The XRD of poly(hydroxamic acid) 3 is presented in Figure 7biii, where two new peaks were observed at  $30 \text{ and } 32^\circ$  along with the disappearance of peaks

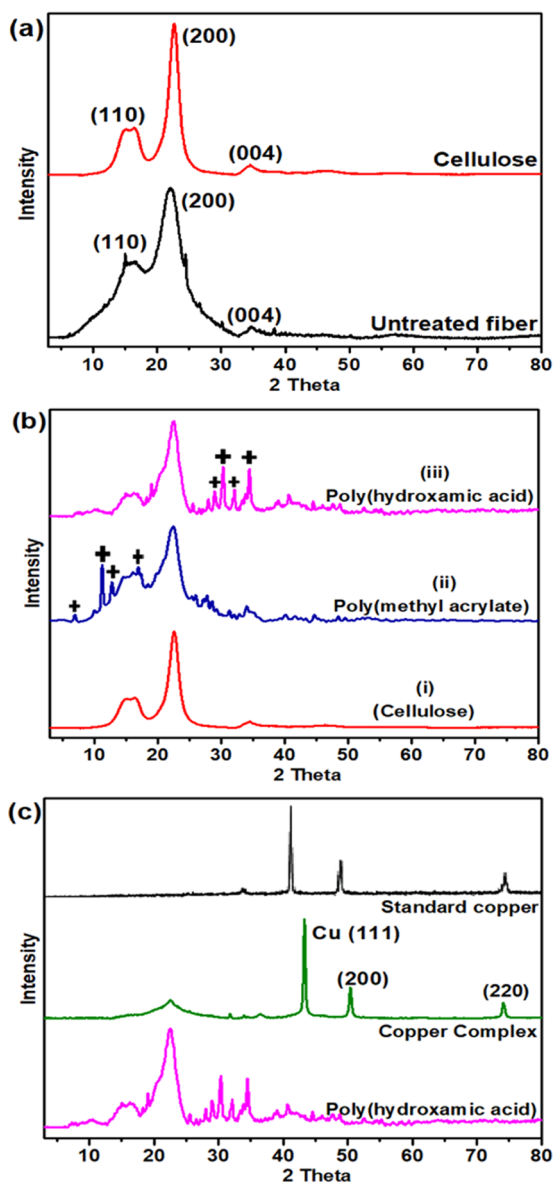


**Figure 6.** XRD spectra of the comparison of (a) untreated pandanus fruit fiber and cellulose 1, (b) poly(methyl acrylate) 2 and poly(hydroxamic acid) 3, and (c) before and after anchoring copper onto poly(hydroxamic acid) 3.

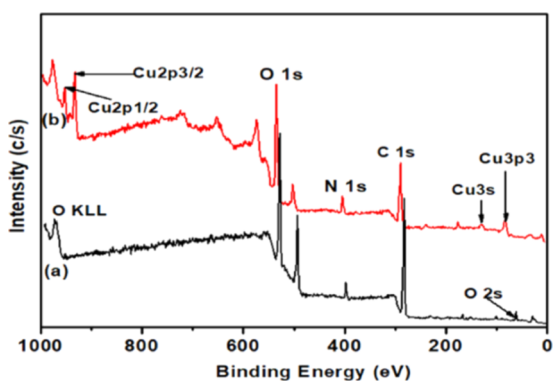


**Figure 7.** Survey scan of XPS for (a) poly(hydroxamic acid) 3 and (b) Cu(II) complex 4.

at 7, 11, 12.8, and 17°, which confirmed the successful conversion of the methyl ester group to the hydroxamic acid functionality.

Before the XRD analysis, Cu(II) complex 4 was reduced to Cu(0) complex. The X-ray diffraction pattern recorded for the copper nanoparticles is shown in Figure 6c. It is found that the XRD pattern has traces of copper oxide at 2θ 36.5°. However, all Bragg's reflections due to metallic Cu(0) are observed at 43.3, 50.4, and 74.1°, corresponding to the miller indices (111), (200), and (220), representing the face-centered cubic structure of copper.<sup>59–62</sup> A broad diffraction peak of cuprite (111) was observed at a diffraction angle of 36.5°. These diffraction peaks were similar in terms of angular positions to those of FCC pure bulk copper crystalline peaks. However, they were relatively broad, as the mean size of the particles was of the order of nanometers.<sup>63</sup> Scherer's equation was used to estimate the mean size of nanoparticles (eq 2).<sup>64</sup> The mean size of copper nanoparticles estimated by XRD data was 33.1 nm.

$$d = \frac{0.9 \lambda}{\beta \cos \theta} \quad (2)$$

where  $d$  is the mean diameter of nanoparticles,  $\lambda$  is the wavelength of an X-ray radiation source, and  $\beta$  is the angular full width at half-maximum (FWHM) of the X-ray diffraction peak at the diffraction angle.

**2.8. X-ray Photoelectron Spectroscopy (XPS) Analysis.** X-ray photoelectron spectroscopy was carried out on an XPS (PHI Quantera II) with an Al 1486.6 eV monochromatic X-ray source at 25.0 W to investigate the complex formation of copper species with poly(hydroxamic acid) 3. The full scan XPS spectra of Cu(II) complex 4 and poly(hydroxamic acid) 3 are shown in Figure 7.

For a full scan, the peaks for binding energies (BEs) were found at 284.0, 399.5, and 531.0 eV, corresponding to the 1s of carbon, nitrogen, and oxygen spectra, respectively; Figure 7a. The binding of Cu(II) was attained by the two new sharp and two new small peaks with BEs of 935.5, 956.0, 125.5, and 80.5 eV, corresponding to Cu 2p<sub>3/2</sub>, Cu 2p<sub>1/2</sub>, Cu 3s, and Cu 3p<sub>3</sub>, respectively (Figure 7b). The Cu(II) ions can be seen in the narrow scan of Cu(II) complex 4 in Figure 8. Two satellite peaks were observed at the BEs of 945 and 965 eV (Figure 8). These two shakeup satellite peaks represent Cu(II) complex 4 exhibiting a d<sup>9</sup> configuration in the ground state of copper.<sup>65</sup> Besides, compared to the narrow scan in Cu(II) complex 4 for Cu(0), these two satellite peaks disappeared. Therefore, we

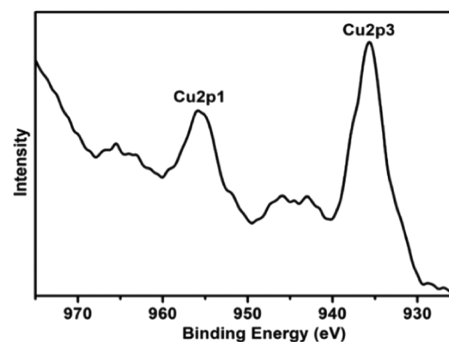


**Figure 8.** Narrow scan of XPS for Cu(II) complex 4 at the copper-binding site.

can confirm that complex 4 had an oxidation state as Cu(II) (see Figure S3).

The core-level O 1s XPS spectra of poly(hydroxamic acid) 3 showed two peaks at the BEs of 530.5 and 532.0 eV, which correspond to the oxygen atoms in the HN–OH and C=O species, respectively (Figure 9a).

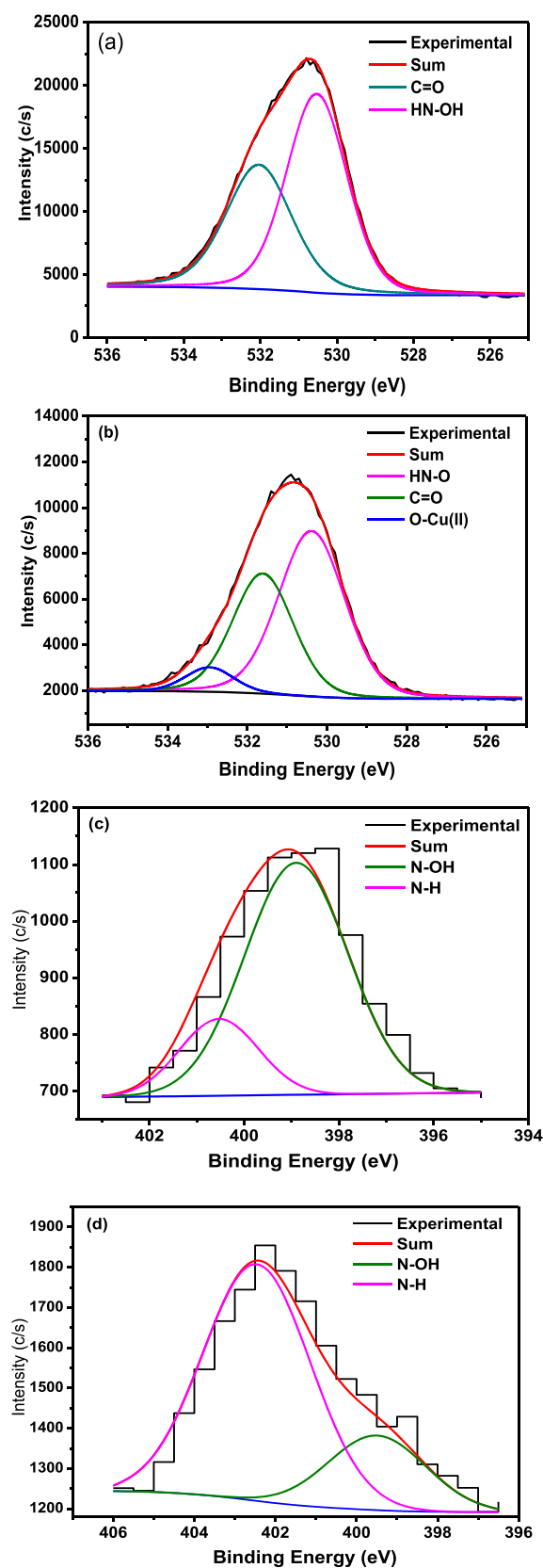
After binding with copper ions, a new peak associated with O 1s of the O–Cu(II) forms a coordinated bond (Figure 9b). For O 1s of the oxygen atoms in O–NH, the BEs of C=O remained the same while a new small peak at 533.0 appeared for O–Cu(II), which confirmed the copper-binding event. In the case of the O 1s core-level spectra, new BE peaks also suggest the coordination between copper and hydroxamic acid for sorption.<sup>66</sup>

The core-level N 1s peak for poly(hydroxamic acid) 3 showed two peaks at BEs of 399.0 and 400.5 eV, corresponding to the nitrogen atoms in the hydroxamic acid functional group N–OH and N–H (Figure 9c), respectively. Binding with copper ions, the N 1s exhibited a small shift to a new peak position with BEs of 399.5 and 402.5 eV due to hydroxamic acid coordination with copper (Figure 9d). This is due to the nitrogen atom in hydroxamic acid possessing lone pair electrons that were donated toward the copper species.<sup>67</sup> The lone pair electrons on the N are donated to the copper metal, resulting in a decrease in the electron density on the N atom, resulting in raised BE peaks.<sup>66</sup>

**2.9. Copper(II)-Catalyzed Ullmann Etherification Reaction.** The functionality of the pandanus cellulose-supported poly(hydroxamic acid) Cu(II) complex 4 was investigated in the Ullmann etherification of phenols and benzyl halides. The initial reaction was performed using phenol (1.2 mmol/0.24 M) and 4-nitrobenzyl bromide (1 mmol/0.2 M) in the presence of 0.015 mol % (15.0 mg) Cu(II) complex 4 and 3.5 mol of K<sub>2</sub>CO<sub>3</sub> in DMF at 80 °C for 8 h. It was observed that Cu(II) complex 4 enhanced the reaction efficiently to obtain the corresponding product 5a with a 65% yield (Table 1, entry 1). Interestingly, a quantitative yield was obtained when the reaction was carried out in the presence of acetonitrile (entry 2). However, the yield was not improved when aqueous ethanol, acetone, and tetrahydrofuran were used as solvents (entries 3–5). We then carried out the reaction by changing the bases (entries 6–9), catalyst loading (entries 10–13), time (entries 14–19), and temperature (entries 20–22). Eventually, we found that  $\pm 5.0$  mg (0.005 mol %) of Cu(II) complex 4, 2 h of reaction time, K<sub>2</sub>CO<sub>3</sub> as the base, acetonitrile, and the reaction temperature of 30 °C were required to carry out the reaction efficiently (Table 1; entry 22).

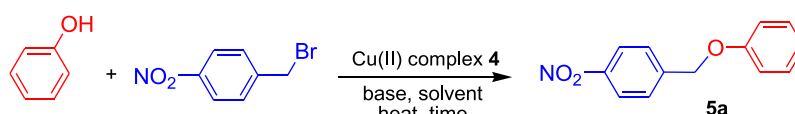
To study the extensive applicability of Cu(II) complex 4 in Ullmann etherification, excess of structurally diverse substituted phenol, benzyl bromide, and phenacyl bromide was used under earlier determined optimized reaction conditions, and the results are summarized in Tables 2 and 3. As illustrated in Table 2, Cu(II) complex 4 efficiently drives the Ullmann reaction toward the desired product in good to excellent yield. Substituted phenol derivatives with both electron-donating and electron-withdrawing groups carried out the Ullmann etherification reaction smoothly with 4-NO<sub>2</sub>/CN/CF<sub>3</sub> substituted benzyl bromide to obtain the respective products in high yields (60–90%) (Table 2).

The catalytic activity of Cu(II) complex 4 toward phenacyl bromide with phenols was then investigated. Interestingly, phenacyl bromide enhanced the Ullmann etherification reaction with substituted phenols in the presence of 0.005



**Figure 9.** O 1s core-level XPS spectra of (a) poly(hydroxamic acid) 3 and (b) Cu(II) complex 4 and N 1s core-level spectra of (c) poly(hydroxamic acid) 3 and (d) Cu(II) complex 4.

mol % Cu(II) complex 4 under the optimized conditions to obtain the corresponding 2-phenoxy-1-phenylethanone (Table

Table 1. Screening of the Ullmann Reaction<sup>a</sup>

type	entry	solvent	base	4 (mg)	temp. (°C)	time (h)	yield (%)	TOF (h <sup>-1</sup> )
solvent	1	DMF	K <sub>2</sub> CO <sub>3</sub>	15 (0.015 mol %)	80	8	65	542
	2	acetonitrile	K <sub>2</sub> CO <sub>3</sub>	15	80	8	99	825
	3	ethanol/H <sub>2</sub> O	K <sub>2</sub> CO <sub>3</sub>	15	80	8	85	708
	4	acetone	K <sub>2</sub> CO <sub>3</sub>	15	60	8	75	625
	5	THF	K <sub>2</sub> CO <sub>3</sub>	15	65	8	57	475
base	6	acetonitrile	KOH	15	80	8	10	83
	7	acetonitrile	CaCO <sub>3</sub>	15	80	8	15	125
	8	acetonitrile	Et <sub>3</sub> N	15	80	8	25	208
	9	acetonitrile	NaOH	15	80	8	5	42
amount of catalyst	10	acetonitrile	K <sub>2</sub> CO <sub>3</sub>	10 (0.01 mol %)	80	8	99	1238
	11	acetonitrile	K <sub>2</sub> CO <sub>3</sub>	5 (0.005 mol %)	80	8	99	2475
	12	acetonitrile	K <sub>2</sub> CO <sub>3</sub>	1 (0.001 mol %)	80	8	90	11 250
	13	acetonitrile	K <sub>2</sub> CO <sub>3</sub>	0	30	8	25	
time	14	acetonitrile	K <sub>2</sub> CO <sub>3</sub>	5	80	6	99	3300
	15	acetonitrile	K <sub>2</sub> CO <sub>3</sub>	5	80	5	99	3960
	16	acetonitrile	K <sub>2</sub> CO <sub>3</sub>	5	80	4	99	4950
	17	acetonitrile	K <sub>2</sub> CO <sub>3</sub>	5	80	3	99	6600
	18	acetonitrile	K <sub>2</sub> CO <sub>3</sub>	5	80	2	99	9900
	19	acetonitrile	K <sub>2</sub> CO <sub>3</sub>	5	80	1.5	99	13 200
temperature	20	acetonitrile	K <sub>2</sub> CO <sub>3</sub>	5	60	1.5	99	13 200
	21	acetonitrile	K <sub>2</sub> CO <sub>3</sub>	5	40	1.5	96	12 800
	22	acetonitrile	K <sub>2</sub> CO <sub>3</sub>	5	30	2	99	9900

<sup>a</sup>Conditions: 4-nitrobenzyl bromide (1 mmol/0.2 M), phenol (1.2 mmol/0.24 M), a catalytic amount of Cu(II) complex 4, and 3 mol equiv of base in 5 mL of solvent. The yield of the product was determined by gas chromatography (GC). The structure of the product was determined by mass spectrometry (MS) and NMR.

3) in a quantitative yield. However, 3-hydroxyphenol provided 60% yield (entry 2) of ether due to the presence of the dihydroxyl group in the benzene ring. It should be noted that phenol had thiol functionality, which efficiently promoted the O-etherification reaction exclusively (entry 6). Therefore, Cu(II) complex 4 can be utilized for the chemoselective O-etherification reaction.

Ullmann etherification of aromatic halides is more challenging compared to benzyl and phenacyl halides.<sup>68</sup> Therefore, we performed the Ullmann etherification reaction under optimum reaction conditions at 60 °C. The Ullmann etherification reaction was enhanced with a variety of substituted phenols and aryl halides to obtain the corresponding ethers up to a 90% yield (Table 4). Aryl chloride showed lower reactivity compared to other halides, and the yield of the ether was significantly affected by the substituent. For example, chlorobenzene provided only 20% of diphenyl ether, whereas 4-cyanochlorobenzene provided the respective product with a 60% yield.

We further investigated the catalytic applicability of Cu(II) complex 4 by synthesizing azoderivatives. When substituted benzyl bromides were treated with ethyl-4-((4-hydroxyphenyl)diazenyl)benzoate under the same reaction conditions, the corresponding azoderivatives 8a–c up to an 88% yield were obtained (Table 5). Therefore, it should be noted that Cu(II) complex 4 is a highly effective catalyst that could be utilized for the synthesis of advance functionalized organic molecules.

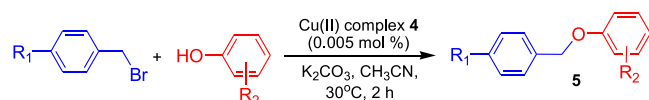
Similarly, phenacyl bromide and ethyl-4-((4-hydroxyphenyl)diazenyl)benzoate also enhanced the Ullmann

reaction to give the respective ether 9 with an 85% yield (Table 6).

The possible mechanism for the pandanus cellulose-supported poly(hydroxamic acid) Cu(II) complex 4-catalyzed reductive O-arylation coupling reaction is shown in Scheme 2.<sup>69,70</sup> The reaction started by (i) adsorption of benzyl halide on the surface of poly(hydroxamic acid) Cu(II) complex 4 through oxidative addition. Therefore, Cu(II) was reduced to Cu(I) to generate the metal active species. (ii) In the presence of K<sub>2</sub>CO<sub>3</sub>, phenol gave a phenoxide anion, which was also absorbed by the copper species. (iii) Finally, diaryl ether was obtained through a reductive elimination process with the regeneration of Cu(II) species, which further undergoes a catalytic reaction.<sup>70,71</sup>

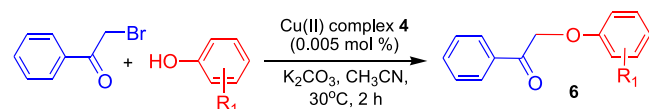
**2.10. Recycling of Cellulose-Supported Poly(hydroxamic Acid) Cu(II) Complex 4.** Catalytic reactivity, stability, and reusability are important features of a true heterogeneous catalyst. Therefore, we concentrated on recycling Cu(II) complex 4 using 0.005 mol% catalytic amount according to Table 1, entry 22. After the first run of the etherification reaction, the reaction mixture was diluted with water and ethyl acetate. The reaction vessel was centrifuged, and Cu(II) complex 4 was recovered by a decantation process. Cu(II) complex 4 was washed with ethyl acetate and acetone, dried at 50 °C, and then was further used in the following run of the reaction without changing the reaction parameter. The pandanus cellulose-supported poly(hydroxamic acid) Cu(II) complex 4 was observed to work efficiently up to seven times without significant loss of its catalytic ability (Figure 10). The only small and negligible loss of catalytic performance was



Table 2. Ullmann Reaction of Benzyl Halides and Phenols<sup>a</sup>


entry	R <sub>1</sub>	R <sub>2</sub>	product	yield (%)	TOF (h <sup>-1</sup> )
1	NO <sub>2</sub>	3-OH	<b>5b</b>	85	8500
2		3-OCH <sub>3</sub>	<b>5c</b>	85	8500
3		3,4-F	<b>5d</b>	99	9900
4		4-CO <sub>2</sub> H	<b>5e</b>	75	7500
5		4-SH	<b>5f</b>	99	9900
6		4-NO <sub>2</sub>	<b>5g</b>	70	7000
7	CN	H	<b>5h</b>	99	9900
8		3-OH	<b>5i</b>	85	8500
9		3-OCH <sub>3</sub>	<b>5j</b>	99	9900
10		3,4-F	<b>5k</b>	99	9900
11		4-CO <sub>2</sub> H	<b>5l</b>	95	9500
12		4-SH	<b>5m</b>	93	9300
13		4-NO <sub>2</sub>	<b>5n</b>	80	8000
14	CF <sub>3</sub>	H	<b>5o</b>	99	9900
15		3-OH	<b>5p</b>	90	9000
16		3-OCH <sub>3</sub>	<b>5q</b>	99	9900
17		3,4-F	<b>5r</b>	99	9900
18		4-CO <sub>2</sub> H	<b>5s</b>	70	7000
19		4-SH	<b>5t</b>	99	9900
20		4-NO <sub>2</sub>	<b>5u</b>	94	9400

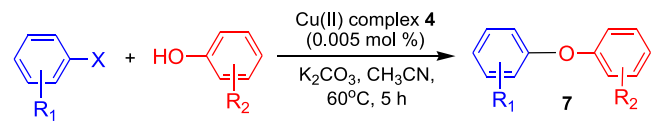
<sup>a</sup>Conditions: benzyl bromide (1 mmol/0.2 M), phenol (1.2 mmol/0.24 M),  $\pm 5.0$  mg (0.005 mol %) of Cu(II) complex **4**, and 3 mol equiv. of K<sub>2</sub>CO<sub>3</sub> in 5 mL of acetonitrile. The yield of the products was determined by GC. The structures of the products were determined by MS and NMR.

Table 3. Ullmann Reaction of Phenacyl Bromide and Phenols<sup>a</sup>


entry	R <sub>1</sub>	product	yield (%)	TOF (h <sup>-1</sup> )
1	H	<b>6a</b>	99	9900
2	3-OH	<b>6b</b>	60	6000
3	3-OCH <sub>3</sub>	<b>6c</b>	96	9600
4	3,4-F	<b>6d</b>	99	9900
5	4-COOH	<b>6e</b>	96	9600
6	4-SH	<b>6f</b>	85	8500
7	4-NO <sub>2</sub>	<b>6g</b>	92	9200

<sup>a</sup>Conditions: phenacyl bromide (1 mmol/0.2 M), phenol (1.2 mmol/0.24 M),  $\pm 5.0$  mg (0.005 mol %) of Cu(II) complex **4**, and 3 mol equiv. of K<sub>2</sub>CO<sub>3</sub> in 5 mL of acetonitrile. The yield of the products was determined by GC. The structures of the products were determined by MS and NMR.

found compared to the first run due to the loss of Cu(II) complex **4** during the decantation and washing process. Further, no significant leaching of copper metal was also confirmed by inductively coupled plasma (ICP) analysis. According to the ICP result, it was ascertained that only a trace amount of copper (the fifth run, <0.10 mol ppm of copper) was leached into the reaction medium after several consecutive runs. Therefore, we believe that Cu(II) complex **4** could be utilized for the production of various ethers on a commercial scale with high yield and regeneration of the catalyst.

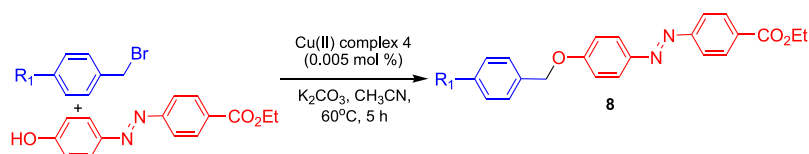
Table 4. Ullmann Reaction of Aryl Halides and Phenols<sup>a</sup>


entry	X	R <sub>1</sub>	R <sub>2</sub>	product	yield (%)	TOF (h <sup>-1</sup> )
1	I	H	H	<b>7a</b>	60	2400
2	I	4-NO <sub>2</sub>	H	<b>7b</b>	77	3080
3	I	4-NH <sub>2</sub>	H	<b>7c</b>	50	2000
4	I	4-CH <sub>3</sub>	H	<b>7d</b>	65	2600
5	I	4-CN	3,4-F	<b>7e</b>	90	3600
6	Br	H	H	<b>7f</b>	55	2200
7	Br	4-NO <sub>2</sub>	H	<b>7g</b>	69	2760
8	Br	4-NH <sub>2</sub>	H	<b>7h</b>	45	1800
9	Br	4-CH <sub>3</sub>	H	<b>7i</b>	50	2000
10	Br	4-CN	3,4-F	<b>7j</b>	82	3280
11	Cl	H	H	<b>7k</b>	20	800
12	Cl	4-NO <sub>2</sub>	H	<b>7l</b>	51	2040
13	Cl	4-NH <sub>2</sub>	H	<b>7m</b>	15	600
14	Cl	4-CH <sub>3</sub>	H	<b>7n</b>	20	800
15	Cl	4-CN	3,4-F	<b>7o</b>	60	2400
16	Br	3-NO <sub>2</sub> , 4-Br	H	<b>7p</b>	67	2680
17	Br	3-NO <sub>2</sub> , 4-Br	3-OCH <sub>3</sub>	<b>7q</b>	75	3000
18	Br	3-NO <sub>2</sub> , 4-Br	3,4-F	<b>7r</b>	65	2600

<sup>a</sup>Conditions: aryl halide (1 mmol/0.2 M), phenol (1.2 mmol/0.24 M),  $\pm 5.0$  mg (0.005 mol %) of Cu(II) complex **4**, and 3 mol equiv. of K<sub>2</sub>CO<sub>3</sub> in 5 mL of acetonitrile. The yield of the products was determined by GC. The structures of products were determined by MS and NMR.

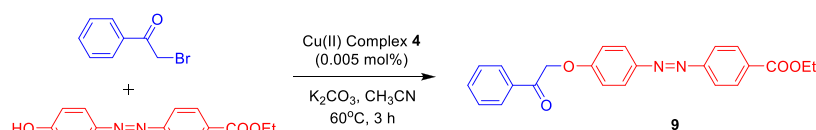
**2.11. Hot Filtration Test of the Ullmann Cross-Coupling Reaction.** To further evaluate the possibility of copper leaching and heterogeneity of the cellulose-supported Cu(II) complex **4** in the reaction medium, we performed a hot filtration experiment (Figure 11). Therefore, we carried out the etherification reaction according to Table 4, entry 5. Two different reactions were performed at 60 °C using 0.005 mol % of Cu(II) complex **4** in acetonitrile. After prolonging the reactions 30 min of the reactions, one of the reaction mixtures was filtered in a glass filter under hot conditions and Cu(II) complex **4** was extracted. The mother liquor (no Cu was detected by the ICP analysis) was further heated under identical conditions. Figure 11 reveals that after removing Cu(II) complex **4** from the reaction mixture, the reaction did not proceed at all (b); however, the other reaction (a) gave a satisfactory yield of the respective ether. Therefore, it is reasonable to consider that the Ullmann etherification reaction proceeded under heterogeneous conditions.

**2.12. Comparison with Other Studies.** Finally, we investigate the virtue of this Cu(II) complex **4** in O-arylation reactions. The simple experimental procedure, reaction conditions, catalyst amounts, and the yield of the product was compared with the reported heterogeneous metal-catalyzed etherification reactions (Table 7). The comparison study revealed that the yield of ethers is generally high; however, it suffers from longer reaction times, strong bases, high temperatures, high catalyst loadings, and low recyclability of the catalyst. Herein, cellulose-supported Cu(II) complex **4** showed remarkable catalytic activity and reusability. It has the advantages not only of high reactivity (0.005 mol %) and good reusability but also of a cost-effective, open-air operating, and eco-friendly catalytic system.

Table 5. Ullmann Reaction of Benzyl Bromides with Azoderivatives<sup>a</sup>

entry	R <sub>1</sub>	product	yield (%)	TOF (h <sup>-1</sup> )
1	-NO <sub>2</sub>	<b>8a</b>	88	5866
2	-CN	<b>8b</b>	80	5333
3	-CF <sub>3</sub>	<b>8c</b>	75	5000

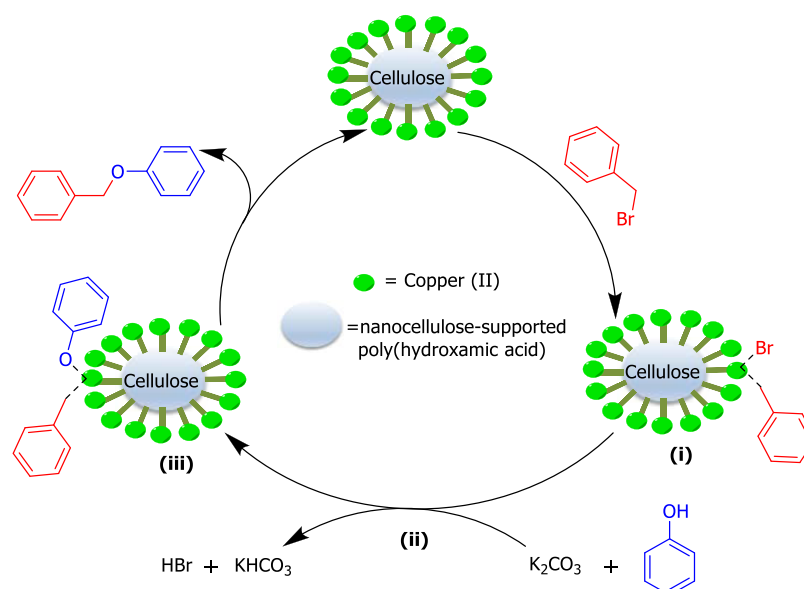
<sup>a</sup>Conditions: benzyl halide (1 mmol/0.2 M), phenol (1.2 mmol/0.24 M),  $\pm$ 5.0 mg (0.005 mol %) of Cu(II) complex 4, and 3 mol equiv of K<sub>2</sub>CO<sub>3</sub> in 5 mL of acetonitrile. The yield of the products was determined by the mass of the purified product. The structures of the products were determined by NMR.

Table 6. Ullmann Reaction of Phenacyl Bromide with Azoderivatives<sup>a</sup>

entry	product	yield (%)	TOF (h <sup>-1</sup> )
1	<b>9</b>	85	5733

<sup>a</sup>Conditions: benzyl halide (1 mmol/0.2 M), phenol (1.2 mmol/0.24 M),  $\pm$ 5.0 mg (0.005 mol %) of Cu(II) complex 4, and 3 mol equiv of K<sub>2</sub>CO<sub>3</sub> in 5 mL of acetonitrile. The yield of the product was determined by the mass of the purified product. The structure of the product was determined by NMR.

Scheme 2. Plausible Mechanism for the Catalytic Synthesis of Ether over Cu(II) Complex 4



### 3. CONCLUSIONS

In summary, we synthesized the pandanus fruit fiber cellulose-supported poly(hydroxamic acid) Cu(II) complex 4, and it was successfully applied in the Ullmann etherification reactions of substituted aryl/benzyl and phenacyl bromide with a variety of phenols. Cu(II) complex 4 showed excellent catalytic activity ( $\pm$ 5.0 mg/0.005 mol%) toward the Ullmann etherification reaction to obtain the respective ethers selectively with excellent yield [benzyl halide (70–99%); aryl halide (20–90%)]. Cu(II) complex 4 can also be utilized for the synthesis of liquid crystal azoderivatives with excellent yield [benzyl bromide (75–88%); phenacyl bromide (85%)]. Moreover,

Cu(II) complex 4 was very stable and showed heterogeneity in the reaction media. Cu(II) complex 4 could be recovered from the reaction mixture easily and reused seven times without loss of its catalytic activity. Hence, Cu(II) complex 4 showed great promise as a reusable and environment-friendly catalyst for practical applications in Ullmann etherification. Therefore, we believe that Cu(II) complex 4 could be utilized to synthesize various ethers on a commercial scale, as well as selectively functionalize thiol-containing phenolic natural products with high yield.

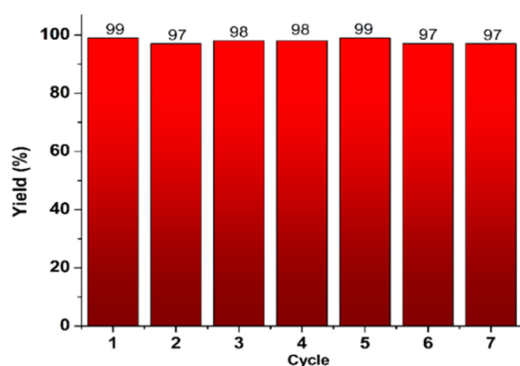


Figure 10. Reusability of Cu(II) complex 4 in O-arylation of phenol with 4-nitrobenzyl bromide.

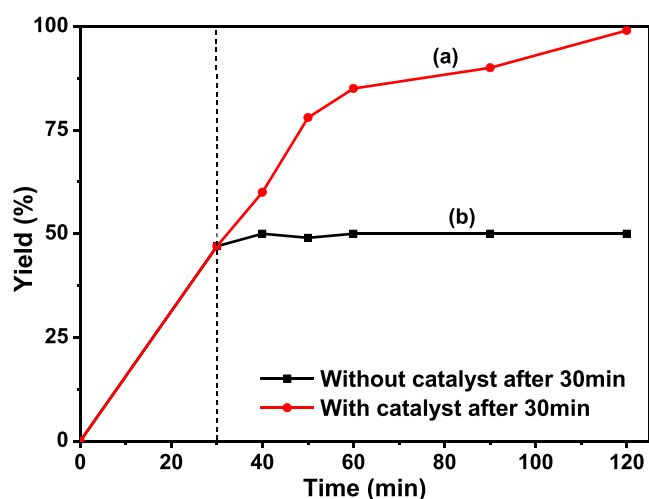


Figure 11. Hot filtration test of the Ullmann reaction (a) in the presence of Cu(II) complex 4 in the whole reaction and (b) on removing Cu(II) complex 4 after 30 min.

## 4. EXPERIMENTAL SECTION

**4.1. Basic Enquiries.** All manipulations were conducted under standard conditions unless otherwise noted. Reagents and solvents were purchased from the Sigma/Merk and were utilized without further purification.  $\text{CuSO}_4$  was purchased from Sigma-Aldrich. A Bruker-600 MHz spectrometer was used to obtain the  $^1\text{H}$  spectra, and TEM was performed on a Tecnai G2 Spirit BioTwin transmission electron microscope.

The  $^1\text{H}$  NMR chemical shift was reported relative to tetramethylsilane (TMS)  $\delta$  0.00 ppm. Inductively coupled plasma optical emission spectrometry (ICP-OES) was performed on a Perkin-Elmer Optima 5300-DV system, and TGA/differential scanning calorimetry (DSC) was performed on a Mettler Toledo TGA/DSC +3 equipment. Gas chromatography-mass spectroscopy was performed on Shimadzu GC-MS-TQ8050 NX equipment. FE-SEM and EDX measured using a JSM-7900F field emission scanning electron microscope, and XRD patterns were measured using a Rigaku automated multipurpose X-ray diffractometer, Central Laboratory, University Malaysia Sabah. XPS was performed on a PHI VersaProbe II. A silica gel 60 F 254 aluminum plate (Merck) was used to perform thin-layer chromatography (TLC) analysis.

**4.2. Extraction of Cellulose (1).** Pandanus fruits were collected from Papar in Sabah, Malaysia. The pandanus fruit fiber was obtained after drying the fruit, as shown in Figure S1. The cellulose pulp was extracted from waste pandanus fruit fibers according to the method described elsewhere.<sup>78,79</sup> The hydrolysis process was carried out in a 1 L Duran bottle in a thermoshaker. The cellulose was hydrolyzed by stirring 5.0 g of the pandanus cellulose pulp in 250 mL of 40% concentrated sulfuric acid (System) for 1.5 h. The resultant product was poured into cold water. The hydrolyzed cellulose 1 was washed with water and centrifuged until the pH became neutral. Product 1 was dried in an oven at 50 °C for 1 day to obtain a constant weight.<sup>80</sup>

**4.3. Graft Copolymerization: Poly(methyl acrylate) (2).** The reaction was carried out in a 1 L three-neck round-bottom flask and fixed with a stirrer and condenser in a thermostat oil bath. The cellulose-supported poly(methyl acrylate) suspension was prepared by stirring 5.0 g of 1 in 500 mL of distilled water overnight. Then, 3 mL of concentrated sulfuric acid was added into the suspension and the reaction was conducted at 75 °C with constant stirring. After being stirred for 5 min, 2.0 g of ceric ammonium nitrate (CAN) (in 12 mL of  $\text{H}_2\text{O}$ ) was added to the mixture and the reaction was continued under a nitrogen atmosphere for 30 min. Purified methyl acrylate (15 mL) was added to the reaction mixture and the resulting suspension was stirred for 5 h under a nitrogen atmosphere. The mixture was cooled to room temperature and the desired product was precipitated from the reaction mixture. The precipitates were rinsed in an aqueous solution of methanol (methanol/ $\text{H}_2\text{O}$  = 4:1 v/v)

Table 7. Comparison of the Cu(II) Complex 4-Catalyzed Ullmann Reaction with Previously Reported Results

entry	type of supported catalyst	catalyst loading	condition	yield (%)	refs
1	chitosan	2.8 mol % Cu, 30.17 mol % Fe	DMSO, 15 h, 120 °C, $\text{K}_2\text{CO}_3$	55–95	71
2	creatin	0.8 mol %	glycerin, 24 h, 80 °C, $\text{K}_2\text{CO}_3$	35–80	72
3	$\text{Fe}_3\text{O}_4$ magnetic nanoparticles	1.25 mol %	$\text{H}_2\text{O}$ , 35 min–18 h, reflux, KOH	I: 84–97 Br: 62–91 Cl: 38–86	73
4	mesoporous graphitic carbon nitrile (mpg- $\text{C}_3\text{N}_4$ )	5.67 mol %	DMF, 5 h, 110 °C, $\text{K}_2\text{CO}_3$	I: 75–90 Br: 77–82 Cl: 33–40	74
5	Isatin@4-(aminomethyl) benzoic acid-functionalized (IS-AMBA)	2.00 mol %	DMF, 4 h, 110 °C, $\text{K}_2\text{CO}_3$	I: 21–98 Br: 30–63	75
6	covalent anchoring of the ligand (AS)	7.00 mol %	DMF, 24 h, reflux, $\text{Cs}_2\text{CO}_3$	45–98	76
7	MWCNTs-Met/CuCl	1.30 mol %	DMF, 8–20 h, 80 °C, $\text{K}_2\text{CO}_3$	55–96	77
8	cellulose-supported poly(hydroxamic acid)	0.005 mol %	this study	up to 99	

(Scheme 1) to give poly(methyl acrylate) **2**. Poly(methyl acrylate) **2** was dried in an oven at 55 °C to obtain a constant weight.<sup>67</sup>

#### 4.4. Synthesis of Poly(hydroxamic acid) Ligand (**3**).

The hydroxylamine solution was prepared by dissolving 20.0 g of hydroxylammonium chloride (NH<sub>2</sub>OH·HCl) in 500 mL of aqueous methanol (methanol/H<sub>2</sub>O = 5:1). To this solution, 60% sodium hydroxide was added until the pH reached 13, and the resulting sodium chloride salt was removed by filtration. This solution was transferred to 10.0 g of poly(methyl acrylate) **2**, and the reaction mixture was stirred at 80 °C for 6 h. The resultant poly(hydroxamic acid) **3** was filtered out from the solution and washed with methanol (Scheme 1). Poly(hydroxamic acid) **3** was treated with 100 mL of 0.1 M hydrochloric acid (HCl) in methanol for 5 min. Finally, the cellulose-supported poly(hydroxamic acid) **3** was filtered using a glass filter and washed several times with acetone. Then, poly(hydroxamic acid) **3** was dried in an oven at 55 °C to obtain a constant weight.<sup>47,81</sup>

#### 4.5. Preparation of Cu(II)@poly(hydroxamic acid) (**4**).

An aqueous solution of copper(II) sulfate (9.33 g, 1 M, 50 mL of distilled water) was added to a stirred suspension of poly(hydroxamic acid) **3** (10.0 g) in 50 mL of pH 6 buffer solution at standard conditions. Colorless poly(hydroxamic acid) **3** instantly changed to green Cu(II) complex **4** (Figure 12). The mixture was filtrated using a glass filter; washed with

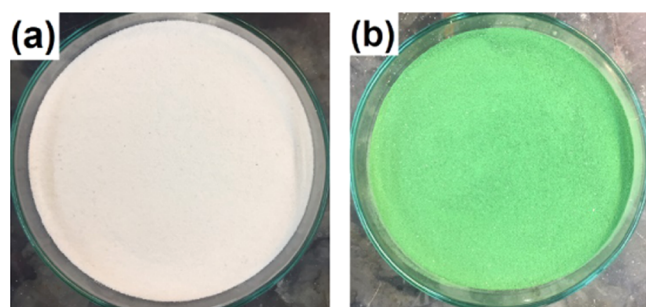


**Figure 12.** (a) Poly(hydroxamic acid) **3** before copper anchoring and (b) poly(hydroxamic acid) **3** after complexation with copper (Cu(II) complex **4**).

ammonium chloride, water, and methanol; and dried at 60 °C for 1 day. The ICP-OES analysis was carried out to estimate the quantity of copper in Cu(II) complex **4** (Scheme 1). From the ICP-OES analysis, it was observed that 0.01 mmol/g copper was present in Cu(II) complex **4**.

## ■ ASSOCIATED CONTENT

### Supporting Information

The Supporting Information is available free of charge at <https://pubs.acs.org/doi/10.1021/acsomega.0c05840>.

Mass and <sup>1</sup>H NMR spectra of compounds **5a–u** (Figures S4–S24), **6a–g** (Figures S25–S31), **7a–r** (Figures S32–S39), **8a–c** (Figures S40–S42), and **9** (Figure S43) (PDF)

## ■ AUTHOR INFORMATION

### Corresponding Author

MdLutfur Rahman – Faculty of Science and Natural Resources, University Malaysia Sabah, 88400 Kota Kinabalu,

Sabah, Malaysia; [orcid.org/0000-0002-9294-453X](https://orcid.org/0000-0002-9294-453X);  
Email: [lutfur73@gmail.com](mailto:lutfur73@gmail.com)

## Authors

**Choong Jian Fui** – Faculty of Science and Natural Resources, University Malaysia Sabah, 88400 Kota Kinabalu, Sabah, Malaysia

**Tang Xin Ting** – Faculty of Science and Natural Resources, University Malaysia Sabah, 88400 Kota Kinabalu, Sabah, Malaysia

**Mohd Sani Sarjadi** – Faculty of Science and Natural Resources, University Malaysia Sabah, 88400 Kota Kinabalu, Sabah, Malaysia

**Zarina Amin** – Biotechnology Research Institute, University Malaysia Sabah, 88400 Kota Kinabalu, Sabah, Malaysia

**Shaheen M. Sarkar** – Department of Chemical Sciences, Bernal Institute, University of Limerick, Limerick V94 T9PX, Ireland

**Baba Musta** – Faculty of Science and Natural Resources, University Malaysia Sabah, 88400 Kota Kinabalu, Sabah, Malaysia

Complete contact information is available at:  
<https://pubs.acs.org/10.1021/acsomega.0c05840>

## Author Contributions

The manuscript was written through the contributions of all authors. All authors have given approval to the final version of the manuscript.

## Notes

The authors declare no competing financial interest.

## ■ ACKNOWLEDGMENTS

The generous support of the Skim UMSGreat, funding no. GUG0382-1/2019, initiated by the University Malaysia Sabah is gratefully acknowledged.

## ■ REFERENCES

- (1) Carroll, M. P.; Guiry, P. J. P,N ligands in asymmetric catalysis. *Chem. Soc. Rev.* **2014**, *43*, 819–833.
- (2) Bariwal, J.; Van der Eycken, E. C–N bond forming cross-coupling reactions: an overview. *Chem. Soc. Rev.* **2013**, *42*, 9283–9303.
- (3) Enugala, R.; Carvalho, L. C. R.; Dias Pires, M. J.; Marques, M. M. B. Stereoselective Glycosylation of Glucosamine: The Role of the N-Protecting Group. *Chem. Asian J.* **2012**, *7*, 2482–2501.
- (4) Puthiaraj, P.; Ahn, W.-S. Synthesis of copper nanoparticles supported on a microporous covalent triazine polymer: an efficient and reusable catalyst for O-arylation reaction. *Catal. Sci. Technol.* **2016**, *6*, 1701–1709.
- (5) Beletskaya, I. P.; Cheprakov, A. V. Copper in cross-coupling reactions: The post-Ullmann chemistry. *Coord. Chem. Rev.* **2004**, *248*, 2337–2364.
- (6) Khan, F.; Dlugosch, M.; Liu, X.; Banwell, M. G. The Palladium-Catalyzed Ullmann Cross-Coupling Reaction: A Modern Variant on a Time-Honored Process. *Acc. Chem. Res.* **2018**, *51*, 1784–1795.
- (7) Egorova, K. S.; Ananikov, V. P. Toxicity of Metal Compounds: Knowledge and Myths. *Organometallics* **2017**, *36*, 4071–4090.
- (8) Taherinia, Z.; Ghorbani-Choghmarani, A. Cu(I)-PNF, an organic-based nanocatalyst, catalyzed C–O and C–S cross-coupling reactions. *Can. J. Chem.* **2019**, *97*, 46.
- (9) Dong, Y.; Bi, J.; Zhang, S.; Zhu, D.; Meng, D.; Ming, S.; Qin, K.; Liu, Q.; Guo, L.; Li, T. Palladium supported on N-Heterocyclic carbene functionalized hydroxyethyl cellulose as a novel and efficient catalyst for the Suzuki reaction in aqueous media. *Appl. Surf. Sci.* **2020**, *531*, No. 147392.

- (10) Dong, Y.; Bi, J.; Zhu, D.; Meng, D.; Ming, S.; Guo, W.; Chen, Z.; Liu, Q.; Guo, L.; Li, T. Functionalized cellulose with multiple binding sites for a palladium complex catalyst: synthesis and catalyst evaluation in Suzuki–Miyaura reactions. *Cellulose* **2019**, *26*, 7355–7370.
- (11) Ye, R.-P.; Lin, L.; Chen, C.-C.; Yang, J.-X.; Li, F.; Zhang, X.; Li, D.-J.; Qin, Y.-Y.; Zhou, Z.; Yao, Y.-G. Synthesis of robust MOF-Derived Cu/SiO<sub>2</sub> catalyst with low copper loading via sol–gel method for the dimethyl oxalate hydrogenation reaction. *ACS Catal.* **2018**, *8*, 3382–3394.
- (12) Xu, Y.; Shi, X.; Hua, R.; Zhang, R.; Yao, Y.; Zhao, B.; Liu, T.; Zheng, J.; Lu, G. Remarkably catalytic activity in reduction of 4-nitrophenol and methylene blue by Fe<sub>3</sub>O<sub>4</sub>@ COF supported noble metal nanoparticles. *Appl. Catal., B* **2020**, *260*, No. 118142.
- (13) Drabina, P.; Svoboda, J.; Sedláč, M. Recent Advances in C–C and C–N Bond Forming Reactions Catalysed by Polystyrene-Supported Copper Complexes. *Molecules* **2017**, *22*, No. 865.
- (14) Dong, M.; Pan, Z.; Peng, Y.; Meng, X.; Mu, X.; Zong, B.; Zhang, J. Selective acetylene hydrogenation over core–shell magnetic Pd-supported catalysts in a magnetically stabilized bed. *AIChE J.* **2008**, *54*, 1358–1364.
- (15) Shang, H.; Liu, C.; Xu, Y.; Qiu, J.; Wei, F. States of carbon nanotube supported Mo-based HDS catalysts. *Fuel Process. Technol.* **2007**, *88*, 117–123.
- (16) Zheng, J.; Chen, Z.; Fang, J.; Wang, Z.; Zuo, S. MCM-41 supported nano-sized CuO–CeO<sub>2</sub> for catalytic combustion of chlorobenzene. *J. Rare Earths* **2020**, *38*, 933–940.
- (17) Bi, J.; Dong, Y.; Zhu, D.; Guo, W.; Meng, D.; Li, T. PdxCuy decorate hypercrosslinked network: Synthesis and application as efficient catalysts for the reduction of 4-nitrophenol and Suzuki–Miyaura coupling reaction. *Appl. Surf. Sci.* **2019**, *495*, No. 143584.
- (18) Meng, D.; Bi, J.; Dong, Y.; Hao, B.; Qin, K.; Li, T.; Zhu, D. Salen-based hypercrosslinked polymer-supported Pd as an efficient and recyclable catalyst for C–H halogenation. *Chem. Commun.* **2020**, *56*, 2889–2892.
- (19) Bi, J.; Dong, Y.; Meng, D.; Zhu, D.; Li, T. The study and application of three highly porous hyper-crosslinked catalysts possessing similar catalytic centers. *Polymer* **2019**, *164*, 183–190.
- (20) Vijaya, Y.; Popuri, S. R.; Boddu, V. M.; Krishnaiah, A. Modified chitosan and calcium alginate biopolymer sorbents for removal of nickel (II) through adsorption. *Carbohydr. Polym.* **2008**, *72*, 261–271.
- (21) Kamal, T.; Khan, M. S. J.; Khan, S. B.; Asiri, A. M.; Chani, M. T. S.; Ullah, M. W. Silver nanoparticles embedded in gelatin biopolymer hydrogel as catalyst for reductive degradation of pollutants. *J. Polym. Environ.* **2020**, *28*, 399–410.
- (22) Djoković, V.; Kršmanović, R.; Božanić, D. K.; McPherson, M.; Van Tendeloo, G.; Nair, P. S.; Georges, M. K.; Radhakrishnan, T. Adsorption of sulfur onto a surface of silver nanoparticles stabilized with sago starch biopolymer. *Colloids Surf., B* **2009**, *73*, 30–35.
- (23) Reddy, K. R.; Rajgopal, K.; Maheswari, C. U.; Kantam, M. L. Chitosan hydrogel: A green and recyclable biopolymer catalyst for aldol and Knoevenagel reactions. *New J. Chem.* **2006**, *30*, 1549–1552.
- (24) Kamal, T.; Ahmad, I.; Khan, S. B.; Asiri, A. M. Bacterial cellulose as support for biopolymer stabilized catalytic cobalt nanoparticles. *Int. J. Biol. Macromol.* **2019**, *135*, 1162–1170.
- (25) Dong, Y.; Wu, X.; Chen, X.; Wei, Y. N-Methylimidazole functionalized carboxymethylcellulose-supported Pd catalyst and its applications in Suzuki cross-coupling reaction. *Carbohydr. Polym.* **2017**, *160*, 106–114.
- (26) Silva, L. S.; Carvalho, J.; Bezerra, R. D. S.; Silva, M. S.; Ferreira, F. J. L.; Osajima, J. A.; Filho, E. C. d. S. Potential of Cellulose Functionalized with Carboxylic Acid as Biosorbent for the Removal of Cationic Dyes in Aqueous Solution. *Molecules* **2018**, *23*, No. 743.
- (27) Dwivedi, A. D.; Dubey, S. P.; Hokkanen, S.; Fallah, R. N.; Sillanpää, M. Recovery of gold from aqueous solutions by taurine modified cellulose: An adsorptive–reduction pathway. *Chem. Eng. J.* **2014**, *255*, 97–106.
- (28) Liu, L.; Xie, J. P.; Li, Y. J.; Zhang, Q.; Yao, J. M. Three-dimensional macroporous cellulose-based bioadsorbents for efficient removal of nickel ions from aqueous solution. *Cellulose* **2016**, *23*, 723–736.
- (29) Rahman, M. L.; Sarkar, S. M.; Yusoff, M. M.; Kulkarni, A. K. D.; Chowdhury, Z. Z.; Ali, M. E. Poly(amidoxime) from Polymer-Grafted Khaya Cellulose: An Excellent Medium for the Removal of Transition Metal Cations from Aqueous Solution. *BioResources* **2016**, *11*, 6780–6800.
- (30) Wu, W.; Wu, P.; Yang, F.; Sun, D.-I.; Zhang, D.-X.; Zhou, Y.-K. Assessment of heavy metal pollution and human health risks in urban soils around an electronics manufacturing facility. *Sci. Total Environ.* **2018**, *630*, 53–61.
- (31) Rahman, M. L.; Sarkar, S. M.; Yusoff, M. M.; Abdullah, M. H. Efficient removal of transition metal ions using poly(amidoxime) ligand from polymer grafted kenaf cellulose. *RSC Adv.* **2016**, *6*, 745–757.
- (32) Rahman, M. L.; Sarkar, S. M.; Yusoff, M. M. Efficient removal of heavy metals from electroplating wastewater using polymer ligands. *Front. Environ. Sci. Eng.* **2016**, *10*, 352–361.
- (33) Ros, S. H. M.; Islam, M. S.; Rahman, M. L.; Rashid, S. S.; Chowdhury, Z. Z.; Ali, M. E.; Sarkar, S. M. Highly Active and Reusable Kenaf Cellulose Supported Bio-Poly (hydroxamic acid) Functionalized Copper Catalysts for C–N Bond Formation Reactions. *BioResources* **2017**, *12*, 882–898.
- (34) Rajender Reddy, K.; Kumar, N. S.; Surendra Reddy, P.; Sreedhar, B.; Lakshmi Kantam, M. Cellulose supported palladium(0) catalyst for Heck and Sonogashira coupling reactions. *J. Mol. Catal. A: Chem.* **2006**, *252*, 12–16.
- (35) Xu, Y.; Zhang, L.; Cui, Y. Catalytic performance of cellulose supported palladium complex for Heck reaction in water. *J. Appl. Polym. Sci.* **2008**, *110*, 2996–3000.
- (36) Keshipour, S.; Shojaei, S.; Shaabani, A. Palladium nanoparticles supported on ethylenediamine-functionalized cellulose as a novel and efficient catalyst for the Heck and Sonogashira couplings in water. *Cellulose* **2013**, *20*, 973–980.
- (37) Seyednejhad, S.; Khalilzadeh, M. A.; Zareyee, D.; Sadeghifar, H.; Venditti, R. Cellulose nanocrystal supported palladium as a novel recyclable catalyst for Ullmann coupling reactions. *Cellulose* **2019**, *26*, 5015–5031.
- (38) Goswami, M.; Das, A. M. Synthesis of cellulose impregnated copper nanoparticles as an efficient heterogeneous catalyst for CN coupling reactions under mild conditions. *Carbohydr. Polym.* **2018**, *195*, 189–198.
- (39) Mandal, B. H.; Rahman, M. L.; Rahim, M. H. A.; Sarkar, S. M. Highly Active Kenaf Bio-Cellulose Based Poly(hydroxamic acid) Copper Catalyst for Aza-Michael Addition and Click Reactions. *ChemistrySelect* **2016**, *1*, 2750–2756.
- (40) Bahsis, L.; El Ayouchia, H. B.; Anane, H.; Benhamou, K.; Kaddami, H.; Julve, M.; Stiriba, S.-E. Cellulose-copper as bio-supported recyclable catalyst for the clickable azide-alkyne [3 + 2] cycloaddition reaction in water. *Int. J. Biol. Macromol.* **2018**, *119*, 849–856.
- (41) Hu, P.; Dong, Y.; Wu, X.; Wei, Y. 2-Aminopyridine functionalized cellulose based Pd nanoparticles: An efficient and ecofriendly catalyst for the Suzuki cross-coupling reaction. *Front. Chem. Sci. Eng.* **2016**, *10*, 389–395.
- (42) Dong, Y.; Lai, Y.; Wang, X.; Gao, M.; Xue, F.; Chen, X.; Ma, Y.; Wei, Y. Design and synthesis of amine-functionalized cellulose with multiple binding sites and their application in CC bond forming reactions. *Int. J. Biol. Macromol.* **2019**, *130*, 778–785.
- (43) Wu, C.; Zhang, X.; Wang, X.; Gao, Q.; Li, X. Surface modification of cellulose nanocrystal using succinic anhydride and its effects on poly (butylene succinate) based composites. *Cellulose* **2019**, *26*, 3167–3181.
- (44) Wohlhauser, S.; Delepierre, G.; Labet, M.; Morandi, G.; Thielemans, W.; Weder, C.; Zoppe, J. O. Grafting Polymers from Cellulose Nanocrystals: Synthesis, Properties, and Applications. *Macromol. Macromolecules* **2018**, *51*, 6157–6189.
- (45) Mohy Eldin, M. S.; Abdel Rahman, S.; El Fawal, G. F. Novel immobilized Cu<sup>2+</sup>-aminated poly (methyl methacrylate) grafted

cellophane membranes for affinity separation of His-Tag chitinase. *Polym. Bull.* **2020**, *77*, 135–151.

(46) Eigen, M.; Tamm, K. Sound absorption in electrolytic solutions due to chemical relaxation. *Z. Elektrochem.* **1962**, *66*, 93–121.

(47) Rahman, M. L.; Mandal, B. H.; Sarkar, S. M.; Wahab, N. A. A.; Yusoff, M. M.; Arshad, S. E.; Musta, B. Synthesis of poly (hydroxamic acid) ligand from polymer grafted khaya cellulose for transition metals extraction. *Fibers Polym.* **2016**, *17*, 521–532.

(48) Rahman, M. L.; Mandal, H. B.; Sarkar, S. M.; Kabir, M. N.; Farid, E. M.; Arshad, S. E.; Musta, B. Synthesis of tapioca cellulose-based poly (hydroxamic acid) ligand for heavy metals removal from water. *J. Macromol. Sci., Part A: Pure Appl. Chem.* **2016**, *53*, 515–522.

(49) Kalia, S.; Sabaa, M. W.; Kango, S. Polymer grafting: A Versatile Means to Modify the Polysaccharides. *Polysaccharide Based Graft Copolymers*; Springer, 2013; pp 1–14.

(50) Rajisha, K. R.; Deepa, B.; Pothan, L. A.; Thomas, S. Thermomechanical and spectroscopic characterization of natural fibre composites. *Interface Eng. Nat. Fibre Compos. Maximum Perform.* **2011**, *35*, 241–274.

(51) Rahman, M. L.; Fui, C. J.; Sarjadi, M. S.; Arshad, S. E.; Musta, B.; Abdullah, M. H.; Sarkar, S. M.; O'Reilly, E. J. Poly(amidoxime) ligand derived from waste palm fiber for the removal of heavy metals from electroplating wastewater. *Environ. Sci. Pollut. Res. Int.* **2020**, *27*, No. 34541.

(52) Fernández, M. J.; Fernández, M. D.; Casinos, I.; Guzmán, G. M. Thermal behavior of cellulosic graft copolymers. I. Cotton grafted with vinyl acetate and methyl acrylate. *J. Appl. Polym. Sci.* **1990**, *39*, 2219–2235.

(53) Das, P.; Saikia, C. N.; Dass, N. N. Thermal behavior of some homogeneously polymethyl methacrylate (PMMA)-grafted high  $\alpha$ -cellulose products. *J. Appl. Polym. Sci.* **2004**, *92*, 3471–3478.

(54) Ling, Z.; Wang, T.; Makarem, M.; Santiago Cintrón, M.; Cheng, H. N.; Kang, X.; Bacher, M.; Pothast, A.; Rosenau, T.; King, H.; Delhom, C. D.; Nam, S.; Vincent Edwards, J.; Kim, S. H.; Xu, F.; French, A. D. Effects of ball milling on the structure of cotton cellulose. *Cellulose* **2019**, *26*, 305–328.

(55) Trilokesh, C.; Uppuluri, K. B. Isolation and characterization of cellulose nanocrystals from jackfruit peel. *Sci. Rep.* **2019**, *9*, No. 16709.

(56) Benyahia, A.; Merrouche, A.; Rahmouni, Z. E. A.; Mansour, R.; Serge, W.; Kouadri, Z. Study of the alkali treatment effect on the mechanical behavior of the composite unsaturated polyester-Alfa fibers. *Mech. Ind.* **2014**, *15*, 69–73.

(57) Rehman, N.; de Miranda, M. I. G.; Rosa, S. M. L.; Pimentel, D. M.; Nachtigall, S. M. B.; Bica, C. I. D. Cellulose and Nanocellulose from Maize Straw: An Insight on the Crystal Properties. *J. Polym. Environ.* **2014**, *22*, 252–259.

(58) Carrillo, I.; Mendonça, R. T.; Ago, M.; Rojas, O. J. Comparative study of cellulosic components isolated from different Eucalyptus species. *Cellulose* **2018**, *25*, 1011–1029.

(59) Ramiyadevi, J.; Jeyasubramanian, K.; Marikani, A.; Rajakumar, G.; Rahuman, A. A. Synthesis and antimicrobial activity of copper nanoparticles. *Mater. Lett.* **2012**, *71*, 114–116.

(60) Khanna, P. K.; Gaikwad, S.; Adhyapak, P. V.; Singh, N.; Marimuthu, R. Synthesis and characterization of copper nanoparticles. *Mater. Lett.* **2007**, *61*, 4711–4714.

(61) Mekewi, M. A.; Darwish, A. S.; Amin, M. S.; Eshaq, G.; Bourazan, H. A. Copper nanoparticles supported onto montmorillonite clays as efficient catalyst for methylene blue dye degradation. *Egypt. J. Pet.* **2016**, *25*, 269–279.

(62) Sreeju, N.; Rufus, A.; Philip, D. Microwave-assisted rapid synthesis of Copper nanoparticles with exceptional stability and their multifaceted applications. *J. Mol. Liq.* **2016**, *221*, No. 1008.

(63) Raffi, M.; Mehrwan, S.; Bhatti, T.; Akhter, J.; Hameed, A.; Yawar, W.; Hassan, M. Investigations into the antibacterial behavior of copper nanoparticles against *Escherichia coli*. *Ann. Microbiol.* **2010**, *60*, 75–80.

(64) Smilgies, D.-M. Scherrer grain-size analysis adapted to grazing-incidence scattering with area detectors. *J. Appl. Crystallogr.* **2009**, *42*, 1030–1034.

(65) Wu, C.-K.; Yin, M.; O'Brien, S.; Koberstein, J. T. Quantitative Analysis of Copper Oxide Nanoparticle Composition and Structure by X-ray Photoelectron Spectroscopy. *Chem. Mater.* **2006**, *18*, 6054–6058.

(66) Mandal, B. H.; Rahman, M. L.; Yusoff, M. M.; Chong, K. F.; Sarkar, S. M. Bio-waste corn-cob cellulose supported poly (hydroxamic acid) copper complex for Huisgen reaction: Waste to wealth approach. *Carbohydr. Polym.* **2017**, *156*, 175–181.

(67) Islam, M. S.; Mandal, B. H.; Biswas, T. K.; Rahman, M. L.; Rashid, S. S.; Tan, S.-H.; Sarkar, S. M. Poly (hydroxamic acid) functionalized copper catalyzed C–N bond formation reactions. *RSC Adv.* **2016**, *6*, 56450–56457.

(68) Alabugin, I. V.; Bresch, S.; Manoharan, M. Hybridization Trends for Main Group Elements and Expanding the Bent's Rule Beyond Carbon: More than Electronegativity. *J. Phys. Chem. A* **2014**, *118*, 3663–3677.

(69) Khalilzadeh, M. A.; Keipour, H.; Hosseini, A.; Zareyee, D. KF/Clinoptilolite, an effective solid base in Ullmann ether synthesis catalyzed by CuO nanoparticles. *New J. Chem.* **2014**, *38*, 42–45.

(70) Kazemi, N.; Mahdavi Shahri, M. Magnetically Separable and Reusable CuFe<sub>2</sub>O<sub>4</sub> Spinel Nanocatalyst for the O-Arylation of Phenol with Aryl Halide Under Ligand-Free Condition. *J. Inorg. Organomet. Polym. Mater.* **2017**, *27*, 1264–1273.

(71) Mousavi Mashhadi, S. A.; Kassaei, M. Z.; Eidi, E. Magnetically recyclable nano copper/chitosan in O-arylation of phenols with aryl halides. *Appl. Organomet. Chem.* **2019**, *33*, No. e5042.

(72) Bagheri, S.; Pazoki, F.; Radfar, I.; Heydari, A. Copper(I)-creatine complex on magnetic nanoparticles as a green catalyst for N- and O-arylation in deep eutectic solvent. *Appl. Organomet. Chem.* **2020**, *34*, No. e5447.

(73) Ashraf, M.; Liu, Z.; Peng, W.-X.; Zhou, L. Glycerol Cu(II) Complex Supported on Fe<sub>3</sub>O<sub>4</sub> Magnetic Nanoparticles: A New and Highly Efficient Reusable Catalyst for the Formation of Aryl-Sulfur and Aryl-Oxygen Bonds. *Catal. Lett.* **2019**, *150*, 1128–1141.

(74) Khalili, D.; Rezaei, M.; Koohgard, M. Ligand-free copper-catalyzed O-arylation of aryl halides using impregnated copper ferrite on mesoporous graphitic carbon nitride as a robust and magnetic heterogeneous catalyst. *Microporous Mesoporous Mater.* **2019**, *287*, 254–263.

(75) Khodaei, M. M.; Alizadeh, A.; Haghypour, M. Preparation and characterization of isatin complexed with Cu supported on 4-(aminomethyl) benzoic acid-functionalized Fe<sub>3</sub>O<sub>4</sub> nanoparticles as a novel magnetic catalyst for the Ullmann coupling reaction. *Res. Chem. Intermed.* **2019**, *45*, No. 2727.

(76) Zahedi, R.; Asadi, Z.; Firuzabadi, F. D. Anchored N,O-Cu complex over Fe<sub>3</sub>O<sub>4</sub>@SiO<sub>2</sub> as a highly efficient and reusable catalyst for CO coupling reaction. *Colloids Surf., A* **2019**, *580*, No. 123728.

(77) Akhavan, E.; Hemmati, S.; Hekmati, M.; Veisi, H. CuCl heterogenized on metformine-modified multi walled carbon nanotubes as a recyclable nanocatalyst for Ullmann-type C–O and C–N coupling reactions. *New J. Chem.* **2018**, *42*, 2782–2789.

(78) Jianfui, C.; Sarjadi, M.; Musta, B.; Sarkar, M.; Rahman, M. L. Synthesis of Sawdust-based Poly(amidoxime) Ligand for Heavy Metals Removal from Wastewater. *ChemistrySelect* **2019**, *4*, 2991–3001.

(79) Rahman, M. L.; Sarjadi, M. S.; Arshad, S. E.; Yusoff, M. M.; Sarkar, S. M.; Musta, B. Kenaf cellulose-based poly(amidoxime) ligand for adsorption of rare earth ions. *Rare Met.* **2019**, *38*, 259–269.

(80) Wulandari, W. T.; Rochliadi, A.; Arcana, I. M. Nanocellulose prepared by acid hydrolysis of isolated cellulose from sugarcane bagasse. *IOP Conf. Ser.: Mater. Sci. Eng.* **2016**, *107*, No. 012045.

(81) Mandal, B. H.; Rahman, M. L.; Rahim, M. H. A.; Sarkar, S. M. Highly Active Kenaf Bio-Cellulose Based Poly (hydroxamic acid) Copper Catalyst for Aza-Michael Addition and Click Reactions. *ChemistrySelect* **2016**, *1*, 2750–2756.